Impact of noise on the regulation of intracellular transport of intermediate filaments

Stéphanie Portet, Sandrine Etienne-Manneville, Cécile Leduc, J.C. Dallon

Impact of noise on the regulation of intracellular transport of intermediate filaments

Stéphanie Portet[1,*], Sandrine Etienne-Manneville[2], Cécile Leduc[3], J. C. Dallon[4]

Abstract

Noise affects all biological processes from molecules to cells, organisms and populations. Although the effect of noise on these processes is highly variable, evidence is accumulating which shows natural stochastic fluctuations (noise) can facilitate biological functions. Herein, we investigate the effect of noise on the transport of intermediate filaments in cells by comparing the stochastic and deterministic formalizations of the bidirectional transport of intermediate filaments, long elastic polymers transported along microtubules by antagonistic motor proteins [1, 2]. By numerically exploring discrepancies in timescales and attractors between both formalizations, we characterize the impact of stochastic fluctuations on the individual and ensemble transport. Biologically, we find that noise promotes the collective movement of intermediate filaments and increases the efficiency of its regulation by the biochemical properties of motor-cargo interactions. While stochastic fluctuations reduce the impact of the initial distributions of motor proteins in cells, the number of binding sites and the affinity of motor-cargo interactions are the key parameters controlling transport efficiency and efficacy.

*Corresponding author

Email addresses: Stephanie.Portet@umanitoba.ca (Stéphanie Portet), sandrine.etienne-manneville@pasteur.fr (Sandrine Etienne-Manneville), cecile.leduc@ijm.fr (Cécile Leduc), dallon@math.byu.edu (J. C. Dallon)

[1]Department of Mathematics, University of Manitoba, Winnipeg, MB, Canada.

[2]Cell Polarity, Migration and Cancer Unit, Institut Pasteur, Paris, UMR3691 CNRS. Equipe Labellisée Ligue Contre le Cancer, F-75015, Paris, France.

[3]Present address: Institut Jacques Monod, 15 rue Hélène Brion, 75013 Paris, France.

[4]Department of Mathematics, Brigham Young University, Provo, Utah, USA.

Keywords: Stochastic versus deterministic formalisms, intracellular transport, motor proteins, tug-of-war, intermediate filaments

1. Introduction

Together with actin filaments and microtubules, intermediate filaments (IFs) are essential components of the cytoskeleton. Intermediate filament proteins self-assemble into long elastic filaments organized in networks. Network dynamics and organization regulate IFs' fundamental cellular functions such as stress-absorbtion, cell division and apoptosis, cell migration, signal transduction and mechanotransduction [3]. We have previously shown that intracellular transport of IFs is essential for the dynamic rearrangements of the network and is regulated by intracellular signals (see, for instance, [4, 5]). Post-translational modifications of IF proteins influence the assembly, disassembly, organization and transport of IFs. Microtubule-dependent transport, one of the modes of transport of IFs in cells, is driven by processive motors dynein and kinesin-1 [6, 7, 8, 9], which move in opposite directions on microtubules.

Given the complexity of the *in vivo* study of intermediate filament transport by motor proteins due to inherent experimental limitations, we use a mathematical modelling framework to identify the key parameters influencing IF transport. There has been extensive theoretical work on modelling dynein and kinesin. There are several good review articles which categorize the models into continuum ratchet [10, 11, 12], discrete stochastic models [10, 11], and models which consider conformational changes [12]. There are phenomenological models [13, 14] and structural models [15, 16, 17]. The models that are most closely related to the work here are models which consider ensembles of motors [11, 18, 19, 20, 21, 22]. We are interested in the transport of intermediate filaments and not in the specific details of the molecular motors. Thus, we follow the work of [20, 21] and consider load sharing motors which result in a tug-of-war which may or may not on average be resolved.

Stochastic and deterministic formulations of the bidirectional transport of

long elastic filaments driven by antagonistic motors have been proposed in [1] and [2], respectively. Using the stochastic form, we account for inherent fluctuations in attachment and detachment of motors, which is the intrinsic noise of the system. As we are interested in the transport of an ensemble of filaments, the inherent heterogeneity in motor distributions within the cells is considered, which defines the extrinsic noise of the system and is described by random initial conditions. By comparing stochastic and deterministic formalizations, we investigate here the effect of intrinsic noise.

In both formulations, the cargo, a long elastic filament representing an intermediate filament, is described as a series of nodes connected by springs with the spring constant describing the elastic properties of filaments. Each node is assumed to have a maximal number of binding sites for each type of motor, which can attach and detach with load-dependent *off* rates. Motors attached to the cargo are assumed to be processive. In the stochastic form, two discrete variables describe the number of opposite motors attached to a node at a given time, instead in the deterministic form, continuous variables represent the proportion of occupied binding sites for opposite motors. As a driving mechanism for bidirectional transport by motor proteins of individual IFs, a local tug-of-war is assumed at each node between the opposite motors. Furthermore, the models analyzed in this work consider the drag force and elastic forces between nodes thus extending the tug-of-war model proposed in [20, 21]. The coordination of motors and resolution of tug-of-war at each node along the filament result in motion of the filament. When possible the model is calibrated in an IF context. In absence of quantified data, we have chosen to vary parameters values within biologically plausible ranges.

As observed in cells, both models produce different modes of transport for IFs; dynein-driven retrograde and kinesin-driven anterograde motions that can happen at different speeds [7]. The effects of different types of *off* rates (properties of motors) on filament transport were investigated in both formalisms [1, 2]. Increasing the number of binding sites along the filaments (properties of filaments regulated by post-translational modifications) is shown to increase the

coordination of motors along filaments and influence the transport efficiency [1]. The elastic properties of filaments can also optimize the coordination of motors along the filaments and transport efficiency or change the direction of transport [1, 2]. With the deterministic form, we show that the coordination of motors results from the interplay between the initial conditions, which is related to intracellular context (distribution of motors in cells), and elastic properties of filaments [2].

Biological systems are inherently subject to stochastic fluctuations. Deterministic forms of models when the size of system (number of copies of molecules or individuals) is large are expected to provide an approximation of the average behaviour of their stochastic analogues. However, decreasing the number of copies of molecules or increasing the order or complexity of reactions (nonlinearity) decrease the quality of the approximation of the mean behavior of stochastic processes by deterministic formalism. For instance, extinction in a stochastic logistic model can occur at very long times that is impossible in its deterministic version, which reaches and never moves from a positive equilibrium [23]. Furthermore, it is known that deterministic and stochastic descriptions of chemical reactions can predict different long term responses even in large size systems [24, 25].

Due to inherent stochasticity of motors (intrinsic noise), a more realistic description of the transport of filaments is to use a stochastic formalism. In the context of our study, the maximal number of motors able to attach per node (that is the size of our system) is small and the nonlinear model considered exhibits multistability, in which deterministic approximations might differ from and fail at capturing long-term dynamics of stochastic processes. Here, comparing results obtained with the deterministic and stochastic formalisms of the model, we investigate the general effect of the random fluctuations on the individual and ensemble transport, which is characterized as the average motion (collective motion) of 150 filaments initially attached to different numbers of motors (random initial conditions to describe intracellular heterogenity, extrinsic noise). The strength of motor-cargo interactions (biochemical properties of the

system) is then varied. In cells, one might hypothesize that changes in motor-cargo interactions are regulated by post-translational modifications of cargo, changes in motor processivity (such as increased dynein processivity by dynactin recruitment [26]) or decreased processivity due to microtubule crowding by microtubule-associated-proteins (MAPs) [27, 28]. Thus, using this modelling framework, we address the following questions: What are the general effects of stochastic fluctuations on the speed, direction and collective transport of filaments? Whether the fluctuations cause small or far-reaching changes in the intracellular transport? How modulating the interactions between processive motors and filaments affects the filament's motion and ensemble transport?

2. Method

2.1. Model description

The focus of this model is the motion of individual IFs transported as cargos by motor proteins along microtubules as observed, for instance, in astrocytes [8, 4], neurons [29] and epithelial cells [30]. In vitro, single IFs have been stretched to more than 200% of their resting length without breaking [31, 32]. Therefore, the model of bidirectional transport of individual IFs by motors proteins represents the cargo, a one-dimensional elongated elastic filament, as a series of N nodes connected by springs. At each node, which describes a portion of filament, antagonistic motors, dynein and kinesin, can attach and detach over time. A maximal number of binding sites at each node is accessible at any time for each type of motors, N_D and N_K (Figure 1A). To the best of our knowledge, values for these parameters N_D and N_K stating the maximal numbers of dynein and kinesin attached along a filament are unknown.

A local tug-of war between antagonistic motors is described at nodes where opposing motors act as loads and identical motors share the load equally following [20]. The equation of motion of a node balances viscous forces, forces generated by antagonistic motors and restoring forces due to elastic coupling.

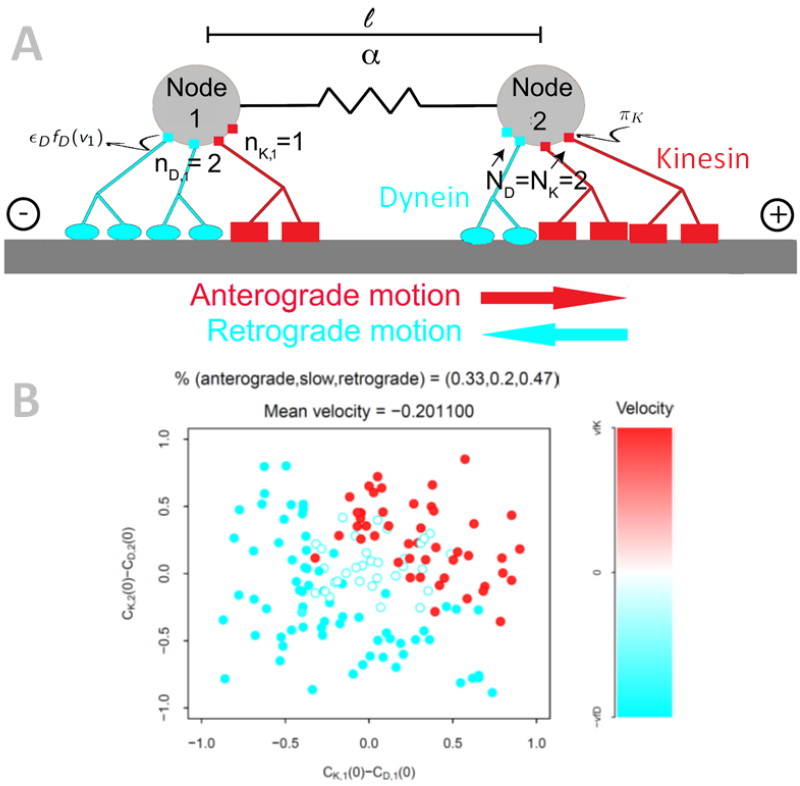

Figure 1: Modelling framework to study the transport of a single and ensemble of intermediate filaments driven by antagonistic motors proteins along microtubules (dark gray rectangle). (A) The cargo, an elastic filament (IF), is composed of two nodes ($N = 2$) connected by a spring with spring constant α and resting length ℓ. On each node, there are two binding sites, which are also the maximal numbers of motors allowed per node, for each type of motors, $N_{\cdot} = 2$. Hence, the cartoon represents an initial setting for a filament (initial conditions): at time $t = 0$, two dyneins and one kinesin are attached to node 1 ($n_{D,1} = 2$ and $n_{K,1} = 1$) and one dynein and two kinesins to node 2 ($n_{D,2} = 1$ and $n_{K,2} = 2$). Over time, motors can detach and attach to nodes if binding sites are available; that changes the balance of forces at nodes and their velocities and so the velocity of the filament. The force-dependent *off* rates from node i, $\epsilon_{\cdot} f_{\cdot}(\cdot)$, is a function of the velocity of the node, v_i. The attachment rates are constant $\pi_{\cdot}$. (B) To study the collective transport, 150 filaments are defined with random initial conditions, which are represented in terms of proportion of occupied binding sites $C_{\cdot,i} = n_{\cdot,i}/N_{\cdot}$ (deterministic representation) instead of the number of motors $n_{\cdot,i}$ attached to a node (stochastic representation) to ease the comparison of results obtained with different values for $N_{\cdot}$. To give a 2D representation of the $3 \times 2 (= N)$-dimensional space, the horizontal (resp. vertical) axis indicates the difference between proportions of binding sites occupied by kinesin $C_{K,1}(0)$ (resp. $C_{K,2}(0)$) and dynein $C_{D,1}(0)$ (resp. $C_{D,2}(0)$) at node 1 (resp. 2) at time $t = 0$. Hence, the position of each dot represents the initial conditions of a filament. Contour (resp. Colour) of dots indicates the direction (resp. velocity) of the filament in long-time: retrograde (cyan) or anterograde (red). Colour-bar indicates velocity values ranging from the no-load velocity of dynein $-v_{fD}$ (cyan) to the no-load velocity of kinesin v_{fK} (red). With the deterministic formalism, the long-time filament velocity is the stable equilibrium velocity reached by both nodes. With the stochastic formalism, the filament velocity is the mean of instantaneous velocities at time T of 50 realizations started with the same initial conditions. Deterministic model results are shown: there exist three locally stable equilibria (multi-stable system), regions roughly delimited by clustered dots of the same colour give an idea of their basin of attraction. The long-time velocities of filaments depend on their initial conditions. The mean velocity of the 150 filaments is -0.201 $\mu m/s$ with 33% of filaments moving anterogradely (positive velocities, via a kinesin-driven transport), 47% retrogradely (negative velocities, via a dynein-driven transport) and 20% of filaments are stalled (there is no winner to the local tug-of-war, both types of motors are still attached to nodes).

For $i \in \{1, \ldots, N\}$, the dynamics of node i is governed by

$$\underbrace{\mu \frac{dx_i}{dt}}_{\text{viscous forces}} = \underbrace{n_{D,i} F_{D,i}}_{\text{forces due to dyneins}} + \underbrace{n_{K,i} F_{K,i}}_{\text{forces due to kinesins}} + \underbrace{F_{res,i}}_{\text{restoring forces}} \tag{1}$$

where $x_i(t) \in \mathbb{R}$ is the position of node i at time t, and $\frac{dx_i}{dt} = v_i$ its velocity. The parameter μ is the drag coefficient. The variables $n_{\cdot,i}$ are the number of dynein ($\cdot = D$) or kinesin ($\cdot = K$) attached to node i at time t and $F_{\cdot,i}$ are the forces from individual motors attached to node i at time t. The restoring forces at time t depend on the spring constant α representing the elastic properties of the filament

$$F_{res,i} = -\alpha \left(r_i(|x_i - x_{i-1}| - \ell) \frac{x_i - x_{i-1}}{|x_i - x_{i-1}|} + l_i(|x_i - x_{i+1}| - \ell) \frac{x_i - x_{i+1}}{|x_i - x_{i+1}|} \right) \tag{2}$$

with ℓ the distance between two adjacent nodes at rest (Figure 1A). The parameters l_i and r_i are equal to 1 for interior nodes; and at the end nodes, $l_1 = r_N = 1$ and $r_1 = l_N = 0$. The spring constant value α is estimated from the Young's modulus of IFs experimentally measured in [33, 34, 35, 36]. Hence, the motion of an individual IF is described by the coupled motion of its N nodes.

In the local tug-of-war (1), single dynein and kinesin motors exert forces to the node they are attached to, in return they experience load forces. Commonly, a load-velocity relationship defines the velocity of a single motor as a function of its load force [37]. For a single dynein, we use

$$v_D(F_{D,i}) = \begin{cases} -v_{fD} & F_{D,i} \leqslant 0 \\ -v_{fD}(1 - F_{D,i}/F_{sD}) & 0 < F_{D,i} < F_{sD} \\ -v_{bD}(1 - F_{D,i}/F_{sD}) & F_{sD} \leqslant F_{D,i} \end{cases}, \tag{3}$$

and for a single kinesin

$$v_K(F_{K,i}) = \begin{cases} v_{bK}(1 - F_{K,i}/F_{sK}) & F_{K,i} \leqslant F_{sK} \\ v_{fK}(1 - F_{K,i}/F_{sK}) & F_{sK} < F_{K,i} < 0 \\ v_{fK} & 0 \leqslant F_{K,i} \end{cases}, \tag{4}$$

where $-v_{fD}$ is the forward or no-load velocity of dynein and v_{fK} is the forward or no-load velocity of kinesin. Similarly, the parameters v_{bD} and $-v_{bK}$ denote the backward velocities of dynein and kinesin. The parameters $F_{s\bullet}$ are the stall forces with $F_{sD} > 0$ and $F_{sK} < 0$.

The model assumes that all motors attached to node i move at the same velocity $v_i = v_D(\cdot) = v_K(\cdot)$, the force-balance (1) must always be satisfied and the motor proteins adjust the force to maintain the velocity relations (3) and (4). Hence, the velocity of a single motor attached to node i depends on the force on that motor, which by the force-balance follows

$$-n_{K,i}F_{K,i} - n_{D,i}F_{D,i} + F_{res,i} - \mu v_i = 0. \tag{5}$$

Therefore, the node velocity v_i and motor forces $F_{\bullet,i}$ are solved explicitly by combining (5), $v_i = v_D(F_{D,i})$ and $v_i = v_K(F_{K,i})$ with $v_D(F_{D,i})$ and $v_K(F_{K,i})$ defined in (3) and (4). The maximum force generated by a single motor is the stall force $-F_{s\bullet}$. As $v_D(\cdot)$ and $v_K(\cdot)$ are piecewise functions, several cases are considered and four regimes are defined. If $F_{res,i} - n_{K,i}F_{sK} < 0$ then the force on the dynein will be negative (when the load is negative, the dynein may oppose the load to adjust the velocity to the no-load velocity), node i moves at the no-load velocity of dynein $-v_{fD}$. When $-n_{K,i}F_{sK} - n_{D,i}F_{sD} + F_{res,i} \leqslant 0$, the node velocity v_i is negative; dynein wins and node i moves to the left. On the other hand, if $-n_{K,i}F_{sK} - n_{D,i}F_{sD} + F_{res,i} \geqslant 0$, the node velocity v_i is positive; kinesin wins the tug-of-war and node i moves to the right. When $F_{res,i} - n_{D,i}F_{sD} > 0$ then the force on the kinesin molecules is positive (when the load is positive, kinesin may oppose the load to adjust the velocity to the no-load velocity), node i moves at the no-load velocity of kinesin v_{fK}. Therefore, the velocity of node

i at time t is defined over four different regimes

$$v_i = \begin{cases} -v_{fD} < 0 & F_{res,i} < n_{K,i}F_{sK} \\ \dfrac{n_{K,i}F_{sK} + n_{D,i}F_{sD} - F_{res,i}}{n_{K,i}F_{sK}/v_{bK} - n_{D,i}F_{sD}/v_{fD} - \mu} < 0 & n_{K,i}F_{sK} \leqslant F_{res,i} < n_{K,i}F_{sK} + n_{D,i}F_{sD} \\ \dfrac{n_{K,i}F_{sK} + n_{D,i}F_{sD} - F_{res,i}}{n_{K,i}F_{sK}/v_{fK} - n_{D,i}F_{sD}/v_{bD} - \mu} > 0 & n_{K,i}F_{sK} + n_{D,i}F_{sD} \leqslant F_{res,i} \leqslant n_{D,i}F_{sD} \\ v_{fK} > 0 & n_{D,i}F_{sD} < F_{res,i}, \end{cases} \tag{6}$$

as well as the force acting on one dynein attached to node i,

$$F_{D,i} = \begin{cases} \dfrac{n_{K,i}F_{sK}(v_{fD}/v_{bK} + 1) - F_{res,i} - v_{fD}\mu}{-n_{D,i}} & F_{res,i} < n_{K,i}F_{sK} \\ \dfrac{F_{sD}(n_{K,i}F_{sK}(1/v_{bK} + 1/v_{fD}) - F_{res,i}/v_{fD} - \mu)}{n_{K,i}F_{sK}/v_{bK} - n_{D,i}F_{sD}/v_{fD} - \mu} & n_{K,i}F_{sK} \leqslant F_{res,i} < n_{K,i}F_{sK} + n_{D,i}F_{sD} \\ \dfrac{F_{sD}(n_{K,i}F_{sK}(1/v_{bD} + 1/v_{fK}) - F_{res,i}/v_{bD} - \mu)}{n_{K,i}F_{sK}/v_{fK} - n_{D,i}F_{sD}/v_{bD} - \mu} & n_{K,i}F_{sK} + n_{D,i}F_{sD} \leqslant F_{res,i} \leqslant n_{D,i}F_{sD} \\ F_{sD}(1 + v_{fK}/v_{bD}) & n_{D,i}F_{sD} < F_{res,i}, \end{cases} \tag{7}$$

and the force acting on one kinesin attached to node i

$$F_{K,i} = \begin{cases} F_{sK}(1 + v_{fD}/v_{bK}) & F_{res,i} < n_{K,i}F_{sK} \\ \dfrac{F_{sK}(-n_{D,i}F_{sD}(1/v_{bK} + 1/v_{fD}) + F_{res,i}/v_{bK} - \mu)}{n_{K,i}F_{sK}/v_{bK} - n_{D,i}F_{sD}/v_{fD} - \mu} & n_{K,i}F_{sK} \leqslant F_{res,i} < n_{K,i}F_{sK} + n_{D,i}F_{sD} \\ \dfrac{F_{sK}(-n_{D,i}F_{sD}(1/v_{bD} + 1/v_{fK}) + F_{res,i}/v_{fK} - \mu)}{n_{K,i}F_{sK}/v_{fK} - n_{D,i}F_{sD}/v_{bD} - \mu} & n_{K,i}F_{sK} + n_{D,i}F_{sD} \leqslant F_{res,i} \leqslant n_{D,i}F_{sD} \\ \dfrac{-n_{D,i}F_{sD}(v_{fK}/v_{bD} + 1) + F_{res,i} - \mu v_{fK}}{n_{K,i}} & n_{D,i}F_{sD} < F_{res,i}. \end{cases} \tag{8}$$

To summarize, the motor molecules have constant forward and backward speeds. When forces try to pull them faster they will resist the forces to maintain the constant speed until they detach. In turn, the velocity of node i and forces acting on single motors partly depend on the number of motors attached to node i, $n_{D,i}$ and $n_{K,i}$, that vary over time as described below.

As the focus of our model is the motion of cargo, attachment and detachment

events are related to the motor-cargo interactions, hypothesizing that motors are processive. Hence, the attachment and detachment rates used in the present work combine the usual part of attachment/detachment of motors to and from microtubules and the interaction between motors and cargo. Detachments of motors from microtubules are force dependent [38], so the detachment rates or *off* rates take the form of the usual load-dependent functions [18, 39]. Instead, the attachment rates or *on* rates, π_D and π_K, are constant.

For the stochastic version of the model, numbers of dynein and kinesin bound to node i, $n_{D,i}$ and $n_{K,i}$, evolve stochastically over time with

- the effective attachment rate $(N_\bullet - n_{\bullet,i})\pi_\bullet$,
- and the effective detachment rate $\epsilon_\bullet f_\bullet(F_{\bullet,i})n_{\bullet,i}$,

where $\epsilon_\bullet f_\bullet(F_{\bullet,i})$ is the force-dependent *off* rate with $F_{\bullet,i}$ defined by (7) and (8). Kramers' framework is used for the force-dependent part of the *off* rates, $f_\bullet(F_{\bullet,i}) = \exp\left[\frac{|F_{\bullet,i}|}{F_{d\bullet}}\right]$, where the parameter $F_{d\bullet}$ is the detachment force (Table 1). Values for no-load *off* and *on* rates, $\epsilon_\bullet$ and $\pi_\bullet$, are unknown in our context. Other force-dependent function forms can be used; see, for instance, [1, 39]. For stochastic simulations, the $N-$dimensional system formed by (1) is solved numerically and the attachment and detachment events at nodes are determined using a modified Gillespie algorithm; see [1] for details. Hence, the stochastic formalization of the model describes the inherent stochastic nature of attachment and detachment processes of motors from the cargo, which represents the source of the intrinsic noise in the system [40]. The instantaneous velocities of nodes are computed over 50 realizations starting with the same initial conditions. For a realization, the instantaneous velocity of node i is computed as follows $v_i(T) = (x_i(T) - x_i(T - 0.5))/0.5$ with $T \geqslant 0$.

For the deterministic version, real-valued variables are used, which are the proportions $C_{\bullet,i}$ of occupied binding sites for each type of motors at node i on the cargo,

$$C_{\bullet,i} = \frac{n_{\bullet,i}}{N_\bullet}, \quad C_{\bullet,i} \in [0, 1]$$

and their evolution equations are, $i \in \{1, \ldots, N\}$

$$\frac{dC_{\bullet,i}}{dt} = \overbrace{(1 - C_{\bullet,i})\pi_{\bullet}}^{Attachment} - \overbrace{\epsilon_{\bullet} f_{\bullet}(F_{\bullet,i}) C_{\bullet,i}}^{Detachment}.$$

The force $F_{\bullet,i}$ acting on a motor are written as a function of v_i, $F_{\bullet,i} = F_{\bullet,i}(v_i)$, by re-arranging (6) to express $F_{res,i}$ as a function of v_i and substituting back in (7) and (8). Furthermore, to take advantage of rich theories to study the asymptotic behaviour of dynamical systems we transform our system to be able to assess the equilibrium velocities of nodes and characterize the modes of motion of filaments. Differentiating (6) with respect to time while considering the explicit expression for $F_{res,i}$ defined in (2) provides evolution equations for v_i and the model equations for node $i \in \{1, \ldots, N\}$ in the deterministic form. The deterministic model is a $3N-$dimensional system in $C_{K,i}$, $C_{D,i}$ and v_i with $i \in \{1, \ldots, N\}$ defined over four regimes.

For $v_i = -v_{fD}$

$$\begin{aligned}
\frac{dC_{K,i}}{dt} &= (1 - C_{K,i})\pi_K - \epsilon_K f_K(-v_{fD}) C_{K,i}, \quad C_{K,i}(t_0) \in [0,1] \\
\frac{dC_{D,i}}{dt} &= (1 - C_{D,i})\pi_D - \epsilon_D C_{D,i}, \quad C_{D,i}(t_0) \in [0,1] \\
\frac{dv_i}{dt} &= 0, \quad v_i(t_0) = -v_{fD}
\end{aligned} \tag{9}$$

For $-v_{fD} < v_i < 0$

$$\begin{aligned}
\frac{dC_{K,i}}{dt} &= (1 - C_{K,i})\pi_K - \epsilon_K f_K(v_i) C_{K,i}, \quad C_{K,i}(t_0) = k_i \in [0,1] \\
\frac{dC_{D,i}}{dt} &= (1 - C_{D,i})\pi_D - \epsilon_D f_D(v_i) C_{D,i}, \quad C_{D,i}(t_0) = d_i \in [0,1] \\
\frac{dv_i}{dt} &= \frac{\alpha(2v_i - v_{i-1} - v_{i+1}) + (1 - v_i/v_{bK})\frac{dC_{K,i}}{dt} N_K F_{sK} + (1 + v_i/v_{fD})\frac{dC_{D,i}}{dt} N_D F_{sD}}{C_{K,i} N_K F_{sK}/v_{bK} - C_{D,i} N_D F_{sD}/v_{fD} - \mu}, \\
v_i(t_0) &= \frac{k_i N_K F_{sK} + d_i N_D F_{sD}}{k_i N_K F_{sK}/v_{bK} - d_i N_D F_{sD}/v_{fD} - \mu}
\end{aligned} \tag{10}$$

For $0 \leqslant v_i < v_{fK}$

$$\begin{aligned}
\frac{dC_{K,i}}{dt} &= (1-C_{K,i})\pi_K - \epsilon_K f_K(v_i) C_{K,i}, \quad C_{K,i}(t_0) = k_i \in [0,1] \\
\frac{dC_{D,i}}{dt} &= (1-C_{D,i})\pi_D - \epsilon_D f_D(v_i) C_{D,i}, \quad C_{D,i}(t_0) = d_i \in [0,1] \qquad (11) \\
\frac{dv_i}{dt} &= \frac{\alpha(2v_i - v_{i-1} - v_{i+1}) + (1 - v_i/v_{fK})\frac{dC_{K,i}}{dt} N_K F_{sK} + (1 + v_i/v_{bD})\frac{dC_{D,i}}{dt} N_D F_{sD}}{C_{K,i} N_K F_{sK}/v_{fK} - C_{D,i} N_D F_{sD}/v_{bD} - \mu}, \\
v_i(t_0) &= \frac{k_i N_K F_{sK} + d_i N_D F_{sD}}{k_i N_K F_{sK}/v_{fK} - d_i N_D F_{sD}/v_{bD} - \mu}
\end{aligned}$$

For $v_i = v_{fK}$

$$\begin{aligned}
\frac{dC_{K,i}}{dt} &= (1-C_{K,i})\pi_K - \epsilon_K C_{K,i}, \quad C_{K,i}(t_0) \in [0,1] \\
\frac{dC_{D,i}}{dt} &= (1-C_{D,i})\pi_D - \epsilon_D f_D(v_{fK}) C_{D,i}, \quad C_{D,i}(t_0) \in [0,1] \qquad (12) \\
\frac{dv_i}{dt} &= 0, \quad v_i(t_0) = v_{fK},
\end{aligned}$$

where $t_0 \geqslant 0$ is the initial time. Complete details on the derivation of model equations and the characterization of their asymptotic behaviour are given in [2]. In particular, we have shown that all nodes of a filament converge to the same stable equilibrium velocity. The equilibrium velocities satisfy a nonlinear equation and their stability conditions are explicitly expressed as functions of the parameters. The model has multiple stable equilibrium velocities whose values depend on parameters. In each of limiting regimes ($v_i = -v_{fD}$ or v_{fK}), which are positively invariant, there exists a globally asymptotically stable equilibrium. In the intermediate regimes ($-v_{fD} < v_i < v_{fK}$), there exist up to five equilibrium values (up to three locally asymptotically stable points co-existing with up to two unstable saddle points) [2]. For a set of parameter values, the motion of a filament is then determined by its initial conditions. For instance, a filament, which starts with more dynein (resp. kinesin) attached to both nodes moves retrogradely (resp. anterogradely) (see cyan (resp. red) dots at the bottom left (resp. top right) corner of Figure 1B). To obtain the basin of attraction of a stable equilibrium (set of initial conditions whose trajectories converge to

Parameter (unit)	Description	Kinesin	Dynein
$v_{f\cdot}$ (μm/s)	Forward speed of motors	0.83	1
$v_{b\cdot}$ (μm/s)	Backward speed of motors	0.006	0.06
$F_{d\cdot}$ (pN)	Detachment force	3	3
$F_{s\cdot}$ (pN)	Stall force	-6	7
$\epsilon_{\cdot}$ (s^{-1})	Free-load dissociation rate	1	0.25
$\pi_{\cdot}$ (s^{-1})	Attachment rate (base value)	5	1.25
$\kappa_{\cdot} = \epsilon_{\cdot}/\pi_{\cdot}$	Dissociation constant (base value)	0.2	0.2
$N_{\cdot}$	Maximal number of binding sites	4, 16, 32	4, 16, 32
N	Number of nodes	2	
α ($N/\mu m$)	Spring constant	$3.45 \times 10^{-9}/N$	
ℓ (μm)	Rest length of spring	0.5	
μ ($Ns/\mu m$)	Drag coefficient for a node	1.2×10^{-12}	

Table 1: Base parameter values used unless otherwise mentioned for simulations, $\cdot$ is either K or D for kinesin or dynein. Base values for motor parameters follow [20, 21, 38, 42, 43, 44]. The drag coefficient μ is obtained from Eq. (2) in [45]; $\mu = \frac{3\pi\ell\eta}{\ln(\ell/d)+\upsilon}$ where $d = 0.01\mu m$ is the intermediate filament diameter and $\upsilon = 0.312 + 0.565(\ell/d)^{-1} - 0.1(\ell/d)^{-2}$. The cytosol viscosity is set to be $\eta = 1.08$ Pa·s, about 1000 times higher than water.

the stable equilibrium), the deterministic model is numerically solved using the `R` package `deSolve` [41] (Figure 1B).

2.2. Collective motion description

Initial conditions, which are numbers of motors attached to nodes (or proportions of occupied binding sites) at the initial time, can be related to a cellular context illustrating the compartmentalization and heterogeneity of the intracellular environment. In the present work, to assess the collective motion of filaments, we consider an ensemble of 150 filaments of same length, $\ell = 0.5\mu m$. Each filament has $N = 2$ nodes placed at both extremities (Figure 1A). The 150 filaments differ by their random initial conditions; they have different numbers of attached motors at the initial time (Figure 1B). The initial conditions of the 150 filaments, $C_{D,i}(t_0)$ and $C_{K,i}(t_0)$ with $i \in \{1, 2\}$, for the deterministic form are uniformly distributed in $[0, 1]$; and so for the stochastic form $\lfloor C_{D,i}N_D \rceil = n_{D,i}(t_0)$ and $\lfloor C_{K,i}N_K \rceil = n_{K,i}(t_0)$ are uniformly distributed in $\{0, \ldots, N_{\cdot}\}$ with $N_{\cdot} = N_D = N_K$. That set-up is adopted to mimick the variability in spatial and temporal distributions of motor proteins in cells (extrinsic noise) [40], and to account for the dependency of filament motion on initial

conditions. For comparison purposes, the same 150 initial conditions are used throughout this work (Figure 1B).

Then, the ensemble average transport is characterized by the mean velocity of the 150 filaments and their distributions over different regimes of motions. Mean velocity of the 150 filaments is computed using the velocities of individual filaments. For the distributions over different regimes of motion, a filament (initial condition) is categorized as slow S if the final velocity is less than 5% of no-load velocities (final velocity belongs to $[-0.05\times v_{fD}, 0.05\times v_{fK}]$), retrograde R if the final velocity is negative and smaller than $-0.05 \times v_{fD}$, or anterograde A if the final velocity is positive and larger than $0.05 \times v_{fK}$ (Figure 1B).

2.3. Model parameter values

Base values for the parameters used for both formalisms are provided in Table 1. An asymmetric case is chosen for motors; the dynein stall force is assumed to be larger than the kinesin one $|F_{sD}| > |F_{sK}|$ as well as its forward and backward speeds (Table 1). Hence, the dynein stall to detachment force ratio is the largest; dynein is set to be the strongest motor as demonstrated *in vitro* [46, 47].

Recall that in our models, attachment and detachment events are related to the motor-cargo interactions, hypothesizing that motors are processive. In this context, attachment and detachment events may be regulated by modulating interactions between motor proteins and cargo by post-translational modifications of cargo (for instance, phosphorylation), by changing motor activity/processivity via other proteins such as regulating attachments of kinesin to microtubules with kinesin-binding proteins [48, 49], or by intracellular crowding reducing the motor accessibility by cargoes [50]. We have chosen to vary the *on* rates π_D or π_K to determine how regulation of filament attachments with processive motors affects filament transport (Figure 2). Hence, seven values of dissociation constants $\kappa_{\cdot} = \epsilon_{\cdot}/\pi_{\cdot}$ (or affinities, $1/\kappa_{\cdot}$) for each type of motors are considered to study the impact of biochemical properties of motor-cargo interactions on the transport of filaments in cells. Finally, as the number of binding

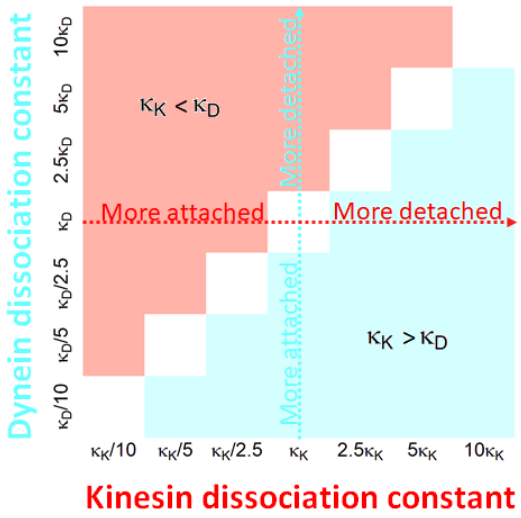

Figure 2: Varying dissociation constants from base values $\kappa_D = \epsilon_D/\pi_D = 0.25/1.25 = 0.2$ and $\kappa_K = \epsilon_K/\pi_K = 1/5 = 0.2$ by varying the *on* rate values. Seven values are used for each dissociation constant, $\kappa./10 = 0.02$, $\kappa./5 = 0.04$, $\kappa./2.5 = 0.08$, $\kappa. = 0.2$, $2.5\kappa. = 0.5$, $5\kappa. = 1$ and $10\kappa. = 2$. Hence, the dynamics are investigated for 49 pairs of dissociation constant values. Regions of higher interaction affinities ($1/\kappa.$) between cargo and dynein are in blue and in red for kinesin. White tiles (anti-diagonal tiles) correspond to same affinities for both types of motors.

sites for motor proteins along IFs is unknown, we consider three different values for the maximal number of motors per node, $N_D = N_K \in \{4, 16, 32\}$.

2.4. Assessing the impact of noise

Comparing the long-time dynamics obtained with each formalism gives the framework to assess the effects of stochastic fluctuations on the transport of intermediate filaments. In the stochastic formalism, the stochastic fluctuations are not an added feature to the system, they are inherent in the model and due to the motors attaching and detaching. They describe an intrinsic noise [40]. A basic random variable represents the number of motors of each type attached to a node. It is a discrete random variable that changes in time depending on the states of the system and is constrained to be an integer between 0 and $N.$. Thus, the parameter $N.$, which is also the size of the system, plays an important role in determining the magnitude of the random fluctuations of the number

of attached motors. As an intrinsic noise, the stochastic fluctuations dominate when the size of the system is small [40]. With more attached motors the tug-of-war between motor types is more easily resolved. Thus, in terms of the filament motion, lower values of $N_\cdot$ result in more random filament motion and higher values result in more stable filament motion. Of course other parameters such as filament length, elasticity, and *off* and *on* rates also affect the stochastic fluctuations [1]. Therefore, the motion of 150 filaments with distinct initial conditions are solved using both the stochastic and deterministic formalism when dissociation constants of motor-cargo interactions $\kappa_\cdot$ vary as described in Figure 2 and the maximal number of motors per node, $N_\cdot$, takes the values 4, 16 and 32.

The long-time behaviour with the deterministic formalism is characterized by the stable equilibrium velocities whose values do not change over time and that are approached by trajectories started from the 150 initial conditions as time grows. With the stochastic formalism, the instantaneous velocity for an initial condition (mean of 50 realizations started with the same initial conditions) is computed at $T=$ 10, 50, 100 and 550 seconds. Several times are considered to detect stationary behaviour in this formalism as we do not have a formal characterization of the long-time dynamics as with the deterministic formalism. The observation timescale is restricted under 10 minutes as phenomena of interest are short-lived in cells (convergence of deterministic dynamics to equilibria occurs under 1 minute).

3. Results

We compare the model responses obtained with the deterministic and stochastic formalisms varying the dissociation constants $\kappa_\cdot$ and number of binding sites $N_\cdot$ to evaluate the effects of the presence of noise on the transport of filaments for distinct biochemical conditions for the motor-filament interactions. The impact on individual filament motions is first deciphered to then elucidate consequences on the ensemble average transport.

Individual filament transport. Figure 3 shows the velocities of 150 filaments as displayed in Figure 1B to assess the individual dynamics and the effects of initial conditions on the filament motion. With the stochastic formalism, the long-time behaviour for some initial conditions differ from the one observed with the deterministic description (Figure 3). With the deterministic formalism (Figure 3A-C), for any pairs of dissociation constants, there are initial conditions resulting in retrograde or anterograde motions. Instead, with the stochastic formalism (Figure 3D-O), there exist pairs of dissociation constants for which only one type of motion is observed; all filaments move retrogradely or anterogradely.

In Figure 3A-C, in absence of noise, initial conditions dictate the final outcome of individual dynamics. Dissociation constants $\kappa_\cdot$ affect equilibrium values, stability conditions and basin of attraction. Depending on the proportions of occupied binding sites at the initial time, filaments move retrogradely (cyan) or anterogradely (red); varying the dissociation constant values modulates proportions of retrograde and anterograde filaments (Figures 3A-C). In presence of noise with a small number of binding sites ($N_\cdot = 4$), comparing panels A to D, G, J and M in Figure 3 shows that the effects of initial conditions on the dynamics of individual filaments are annihilated. Motors with the lowest dissociation constant (or the largest affinity, $1/\kappa_\cdot$) win the tug-of-war.

To understand discrepancies between deterministic and stochastic results, Figure 4 shows the distributions of stable equilibrium velocities reached from the 150 initial conditions with the deterministic formalism and the distributions of the 150 instantaneous velocities at 10 and 550 seconds with the stochastic formalism. When the number of binding sites is small $N_\cdot = 4$ and both types of motors have distinct affinities, distributions of velocities at 10 and 550 seconds do not differ much (orange and blue distributions in off anti-diagonal tiles of Figure 4A); stochastic dynamics converges in a few seconds to distributions centered at one of the locally asymptotically stable equilibria reached in the deterministic dynamics (black dots co-located with white distributions in off anti-diagonal tiles of Figure 4A). Random fluctuations perturb significantly the deterministic equilibrium situations by allowing the trajectories to visit the entire state space

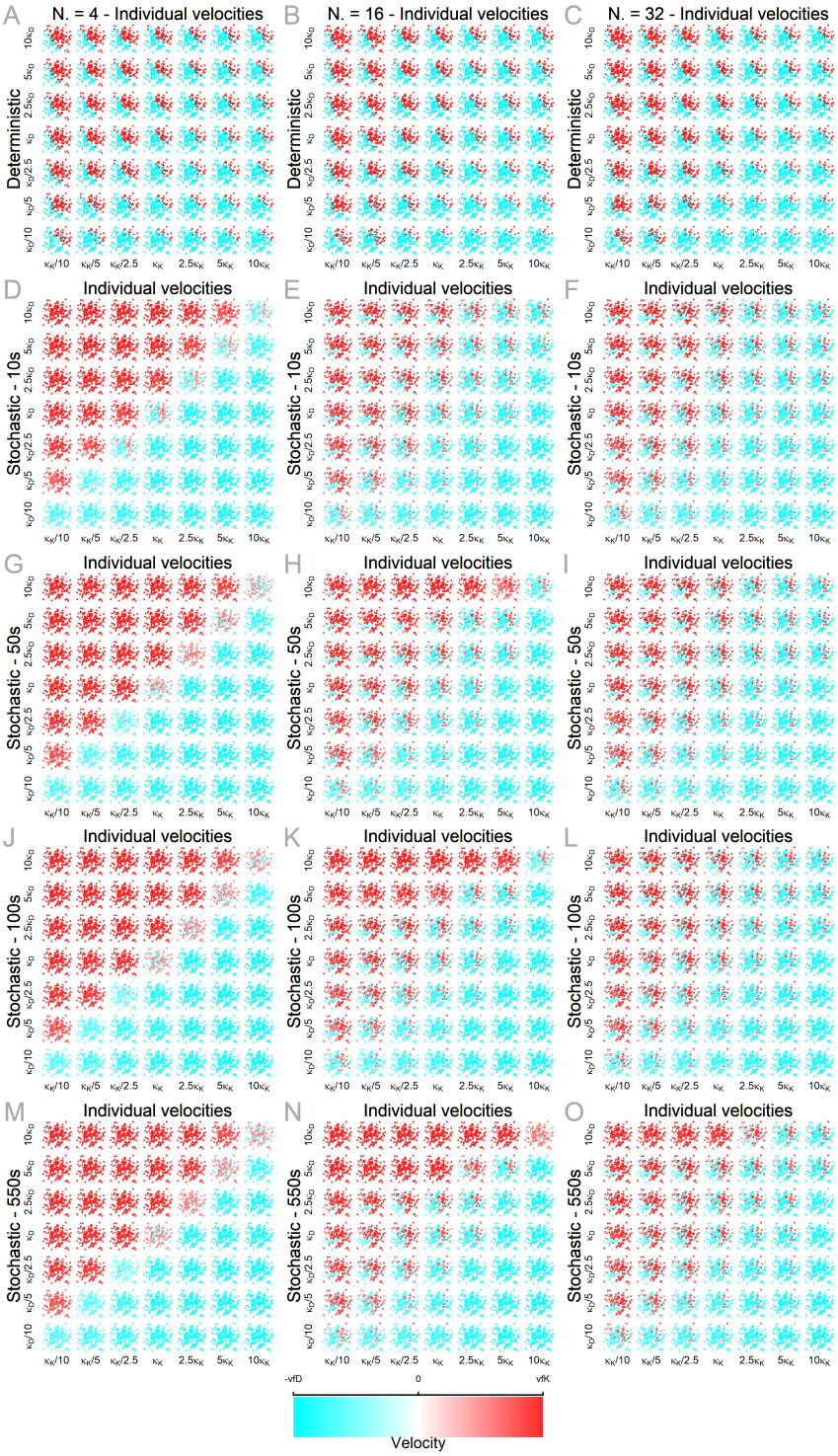

Figure 3: Velocities of the 150 filaments - (Column 1,2,3) $N. = 4, 16, 32$. (Row 1) Deterministic results (Rows 2, 3, 4 and 5) Stochastic results at 10, 50, 100 and 550 seconds. Each 49-tile panel displays the results obtained when dissociation constants of motor-cargo interactions $\kappa.$ vary as in Figure 2. Other parameter values used for simulations are provided in Table 1. In each tile, position of dots indicates the initial conditions of filaments and colors their velocities as in Figure 1B.

(jump to different basins of attraction); finally only one of deterministic locally stable equilibrium velocities is robust to fluctuations (the "global" stable situation – see for example off anti-diagonal tiles of Figure 4A) [51]. Furthermore, when dissociation constants are the same and take large values (short-lived attachments, top right anti-diagonal tile in Figure 4A), the tug-of-war is not resolved when stochastic fluctuations are considered, the stochastic dynamics approach distributions centered at the deterministic small velocity equilibrium (the unstable saddle equilibrium). Increasing the attachment time of motors (going down along the anti-diagonal to bottom left tile in Figure 4A) shifts the center of distributions at 10 and 550 seconds to a negative velocity (tug-of-war is then resolved) whereas, in the deterministic case, a bifurcation has occurred and two more equilibria of small values have appeared (in the bottom left anti-diagonal tile of Figure 4A, the black dot co-located with the white bar at the zero velocity is the superposition of three dots representing three equilibria of very small values; from negative to positive values, the first and last of the three equilibria are unstable saddle points and the equilibrium with the intermediate value is locally asymptotically stable). When dissociation constants are the same for both types of motors and take small values (longer-lived attachments), there exists an extra locally stable equilibrium with the deterministic case, slow motions are then observed resulting from the non-resolution of tug-of-war (white bar at the zero velocity in the bottom left anti-diagonal tile of Figure 4A). This occurs for any value of binding sites (white bar co-located with black dot close to the zero velocity in the bottom left anti-diagonal tile of Figures 4A-C).

When there is a small number of binding sites $N_\cdot = 4$, the effects of stochastic fluctuations are observed from 10 seconds and persist over time (Figures 3D, G, J and M), the stochastic velocities approach rapidly stationary distributions (Figure 4A). With $N_\cdot$ =16 and 32, for some pairs of dissociation constants $\kappa_{\cdot,}$, stochastic distributions of velocities vastly differ from 10 to 550 seconds (orange and blue distributions in Figure 4B-C). For instance, when dissociation constants are the same and take large values with $N_\cdot$ =16, the 550 seconds stochastic velocities (blue distribution in top right anti-diagonal tile of Figure

4B) are approaching the stationary distribution that is centered to the small velocity equilibrium similarly to $N_{\cdot} = 4$. However, at 10 seconds (orange distributions in top right anti-diagonal tile of Figure 4B), the stochastic velocity distributions are centered at locally stable equilibria of the deterministic description; hence, in short timescale, velocity distributions first reach quasi-stationary distributions then stochastic fluctuations continue to perturb the dynamics that will slowly converge to the stationary distribution centered at the unstable equilibrium. With $N_{\cdot} = 32$, at 10 and 550 seconds, the distributions are similar and centered at deterministic locally stable equilibria (orange and blue distributions in top right anti-diagonal tile in Figure 4C). It seems that for several cases of dissociation constant pairs when the number of motor binding sites is high, at least on a timescale relevant for our problem, the stochastic velocities have not converged to a distribution with a small deviation about one velocity yet.

All together, results of individual motions show that stochastic dynamics approach very rapidly distributions with means close to deterministic locally stable equilibria (quasi-stationary distributions); and then stochastic fluctuations continue to perturb dynamics that reach on a slower timescale a stationary distribution centered at one of the deterministic locally stable or unstable equilibria or a value not described by the deterministic formalism [52]. The times to reach these quasi-stationary and stationary distributions vary with parameters and in particular with the maximal number of binding sites per node $N_{\cdot}$. Eventually, the long-time behaviour with the stochastic formalism does not depend on the initial conditions (ergodic system). The presence of noise annihilates eventually the effects of initial conditions. Instead the dynamics of transport is essentially driven by the biochemical properties (motor-cargo interaction affinities). The smaller the maximal number of binding sites, the faster and stronger are the noise effects.

Finally, to quantify the effect of noise on individual dynamics, we categorize the deterministic equilibrium velocity values and the velocities reached at the four time points with stochastic dynamics of the 150 filaments as anterograde (A), slow (S) or retrograde (R). Figure 5 represents the distributions of changes

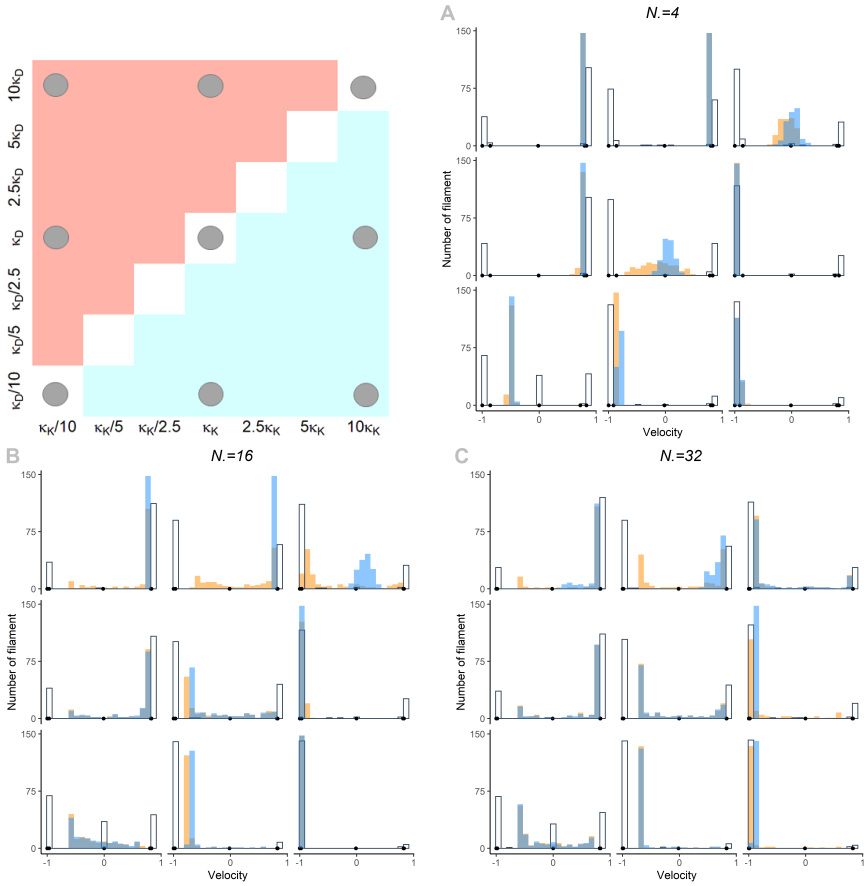

Figure 4: Distributions of the individual velocities reached by the 150 filaments with the deterministic formalism (white bars), with the stochastic formalism after $T = 10$ seconds (in orange) and $T = 550$ seconds (in blue) for the 9 pairs of dissociation constants κ. indicated by grey dots in the first panel. Distributions obtained with N. =4 in (A), 16 in (B) and 32 in (C). Black dots are the (stable and unstable) equilibrium values computed from the deterministic formalism [2]. In the bottom left anti-diagonal tile of (A-C), the black dot located at the zero velocity is in fact the superposition of three dots representing three equilibria of very small values. White bars co-located with black dots indicate the stable equilibria of the deterministic formalism. Results for the 49 pairs of dissociation constants are given in Appendix in Figure A.9.

in regimes of motion of filaments due to the addition of noise. We observe that the presence of noise can slow down ($R \to S$ or $A \to S$, in light colors), speed up ($S \to R$ or $S \to A$, in bright colors), reverse ($R \to A$ or $A \to R$, in dark colors) or unaffect (in grey) the motion of individual filaments. Important changes first appear in regions of high dissociation constants; see, for instance, at 50 seconds for $N_{\cdot} = 16$ (right corner of Figure 5E) and at 550 seconds for $N_{\cdot} = 32$ (right corner of Figure 5L). When both types of motors have distinct biochemical properties (off anti-diagonal tiles in Figure 5), noise can reverse the direction of transport. Slow-down or speed-up of motion are only observed when both types of motors have same biochemical properties (tiles on the anti-diagonal). In particular, for small dissociation constants (lower segment along anti-diagonals in A, D, G or J in Figure 5), the presence of noise speeds up or reverses the direction of filament motion and helps the strongest motor (dynein in this work) to win the tug-of-war. However, with large dissociation constants, the presence of noise stalls filaments (upper segment along anti-diagonals in A, D, G or J in Figure 5) and helps the weakest motor (kinesin in this work).

Ensemble average transport. The collective transport then is assessed in phase diagram style figures representing the mean velocity of 150 filaments and their distribution over different regimes of motion in Figures 6 and 7, respectively. As a first observation, a small mean velocity for the ensemble average transport can correspond to different situations (Figure 6): a population of mainly slow filaments (corresponding to whitish tiles in Figure 6G, J or M and tiles with a majority of S in Figure 7G, J or M), a population of mainly one type (corresponding to light colors tiles in Figure 6J or M and cyan tiles in Figure 7J or M) or a balanced population of anterograde and retrograde filaments (corresponding to light colors tiles in Figure 6N or K and half red and half cyan tiles in Figure 7N or K).

The presence of noise results in the motion of all filaments in the same direction (Figure 7) and in a more efficient transport with an increased mean velocity of the filament ensemble (Figure 6) when motors have different affinities. For

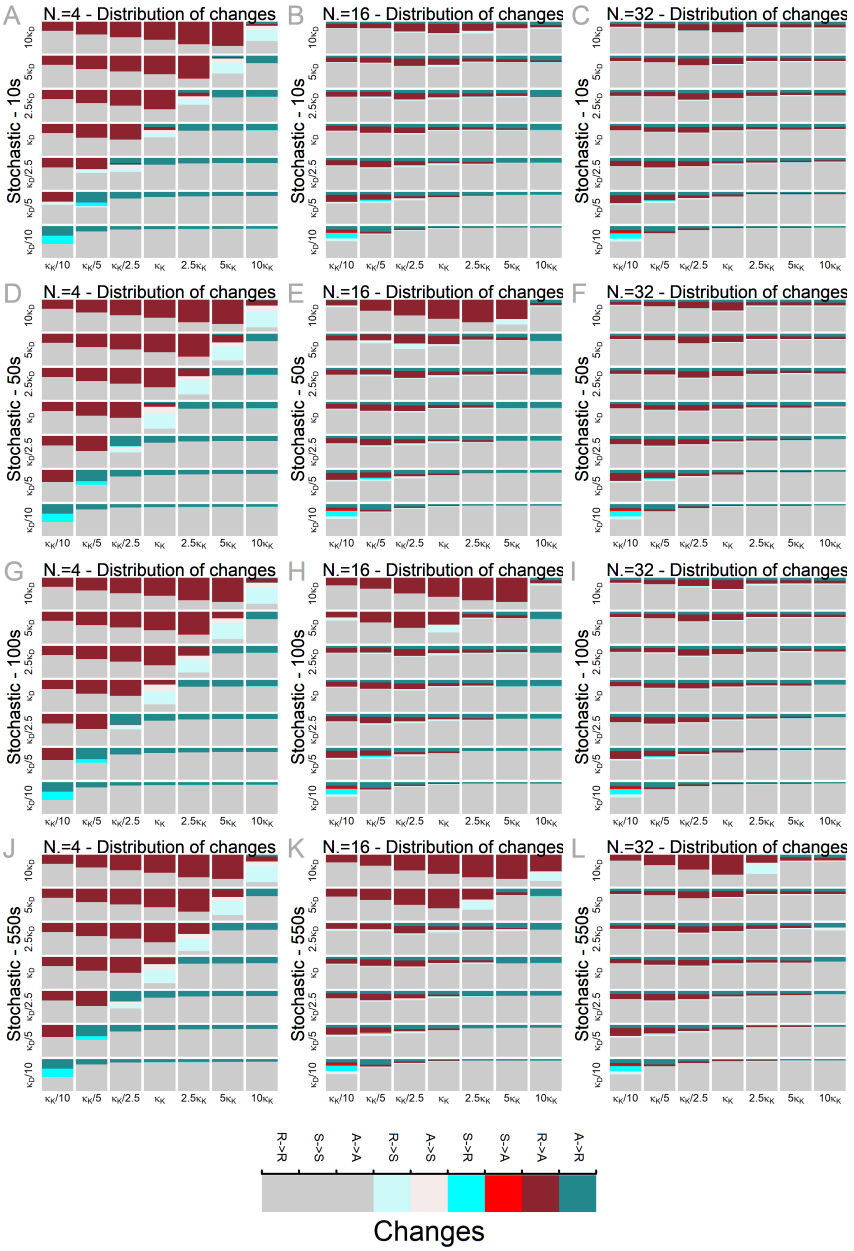

Figure 5: Distributions of changes in regimes of motion of filaments due to addition of noise - Differences between model responses obtained with the deterministic and stochastic formalism (Column 1,2,3) $N. = 4, 16, 32$. (Row 1, 2, 3 and 4) Stochastic at 10, 50, 100 and 550 seconds. In each panel, a tile is a stacked bar-plot showing the proportion of each type of change. No change induced by noise is coded in gray. When the presence of noise slows down the filament, light blue ($R \rightarrow S$) and red ($A \rightarrow S$) are used. When the filament is faster in the stochastic description, bright blue ($S \rightarrow R$) and red ($S \rightarrow A$) are used. When the direction of the filament is changed (opposite direction in deterministic and stochastic descriptions) dark colors are used (dark red for $R \rightarrow A$ and dark blue for $A \rightarrow R$). Parameter values used for simulations are provided in Table 1.

motors with same affinities, the presence of noise slows down the ensemble average transport. Hence, the presence of noise organizes/homogenizes the transport of filaments, the direction of collective motion is determined by the motors with the highest affinity. As previously observed with the individual dynamics, the homogeneization effect of noise on the net transport takes more time when the maximal number of motors per node increases.

Regulating the biochemical properties of motor-cargo interactions allows the regulation of the collective transport. In absence of noise, modulating dissociation constants from their base values (defined as biologically plausible) affects the ensemble transport (Figures 6A-C and and 7A-C). However, changing kinesin or dynein dissociation constants does not have a symmetrical effect with the parameter values considered. To reverse the direction of transport, kinesin dissociation constant must be changed from its base value; changing dynein's constant does not reverse the direction of transport (Figures 6A-C and 7A-C). The presence of noise allows a switch in the transport of filaments between different regimes of motions by varying either kinesin or dynein dissociation constants (Figures 6D-O and 7D-O).

In an attempt to recapitulate the impact of the presence of noise and biochemical properties on the ensemble transport, mean velocities obtained with both the deterministic and stochastic formalisms are plotted as functions of ratios of dissociation constants κ_K/κ_D in Figure 8. That figure aggregates data from Figure 6 for four cases: distinct strong affinities for both motors, one type with a strong affinity and the other with a weak one, distinct weak affinities for both motors and same affinity for both types. With a concomitant regulation of both types of motors (changing simultaneously properties of both motors), the presence of noise always minimizes the differential between dissociation constants allowing a change in the ensemble average transport direction; the intersections of stochastic responses with the horizontal line denoting the change in transport direction in Figure 8 is always closer to zero (same affinities for both motors) than with deterministic responses. Note that with weak affinities motors (G, K and O in Figure 8), varying the ratio of dissociation constants

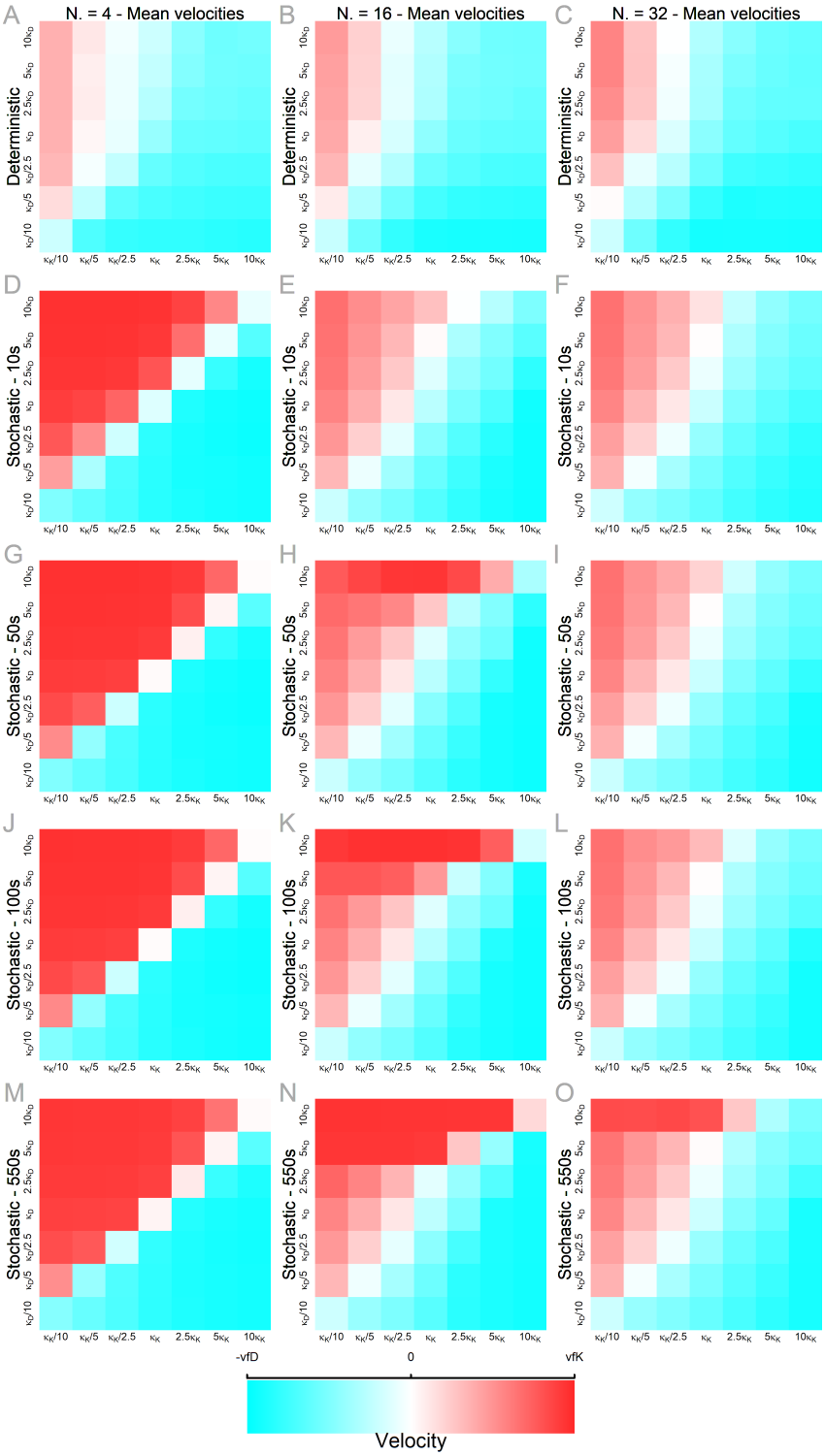

Figure 6: Mean velocities of the 150 filaments - Rows and columns are as in Figure 3 and parameter values used for simulations are provided in Table 1.

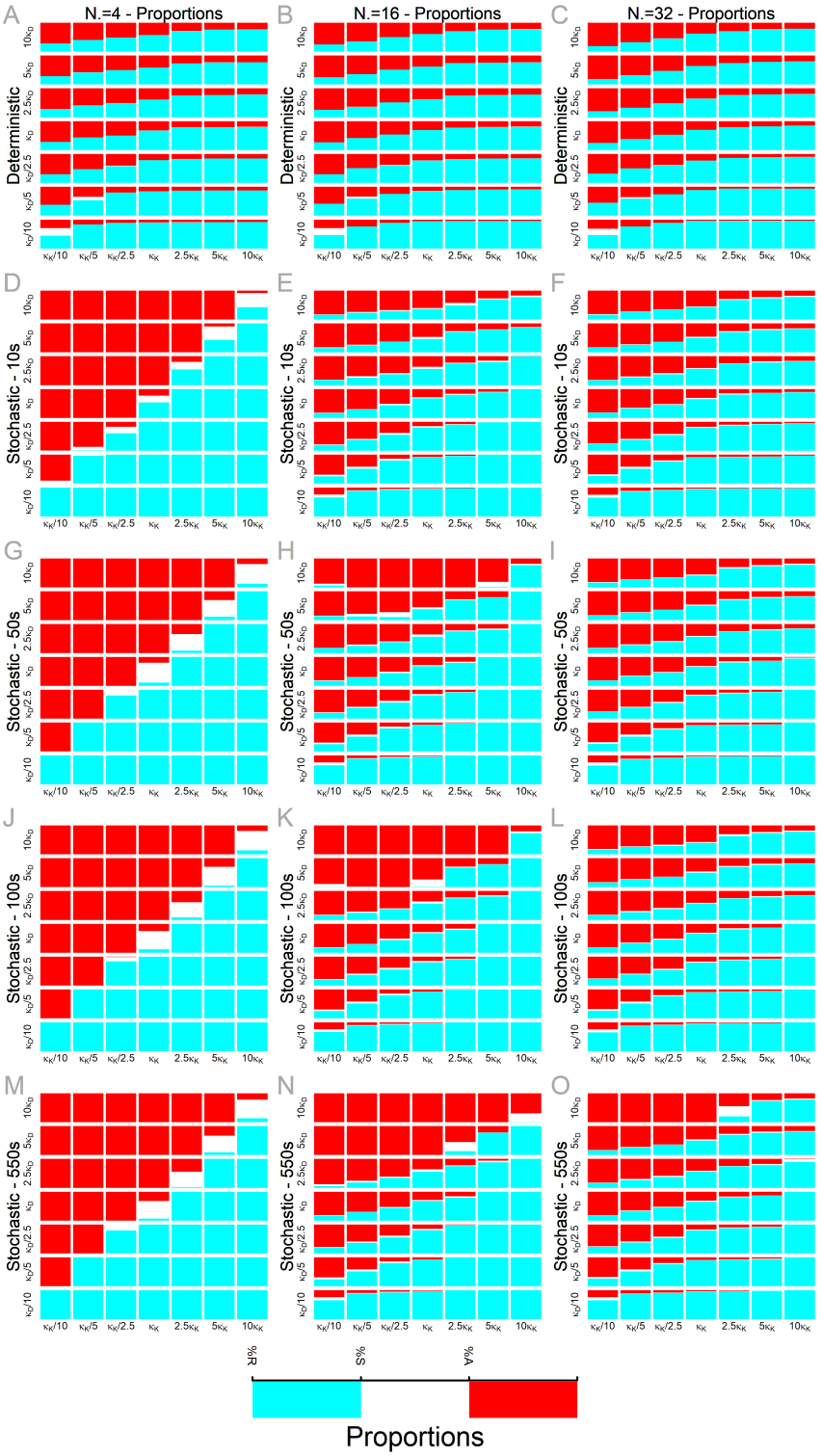

Figure 7: Distributions of filaments over different regimes of motion. In each panel, tiles are stacked bar-plots in which proportions of anterograde (in red), slow (in white) and retrograde (in cyan) filaments are represented. Rows and columns are as in Figure 3 and parameter values used for simulations are provided in Table 1.

does not allow the reversal of transport direction in the deterministic case for the parameters considered. However, the presence of noise allows it, even with large numbers of binding sites ($N_{\cdot} = 32$), it will just take more time. Presence of noise facilitates the regulation of transport by biochemical properties.

With a small number of binding sites ($N_{\cdot} = 4$), the presence of noise rapidly makes the biochemical properties the main driver of the dynamics by annihilating the effects of initial conditions. Differential in dissociation constants sets the direction of net transport (E-H of Figure 8). A slight variation for one type of motors from its affinity base value allows a very efficacious regulation of transport, permitting reversing the collective direction of filaments. When motors have the same biochemical properties and no strong affinities (affinities lower than the base value indicated by the vertical line in Figure 8H and A.10H), the ensemble average transport is very slow, the majority of filaments is stalled; the presence of noise hinders the resolution of the tug-of-war as previously observed.

The presence of noise is the least impactfull for the ensemble average transport when both types of motors have strong affinities (E, I and M in Figures 8 and A.10) and the most influential with weak affinities (G, K and O in Figures 8 and A.10). Systems with large dissociation constants for both types of motors are more prone to perturbations as attached stages are short-lived that makes more sensitive to noise. The smaller the maximal number of motors allowed per node, the stronger and faster the regulation of transport by motor-cargo interactions (Figures 6D-O, 8 and A.10). Strength and timescale of effects of noise on the transport depend on the biochemical properties.

4. Conclusion

We show that the regulation of motor-filament interactions can modulate and reverse the collective transport. The presence of noise (a more realistic description of the stochastic nature of attachment and detachment processes of motors – intrinsic noise) contributes to the regulation of transport by motor-filament interactions diminishing the impact of initial conditions (spatial distributions of

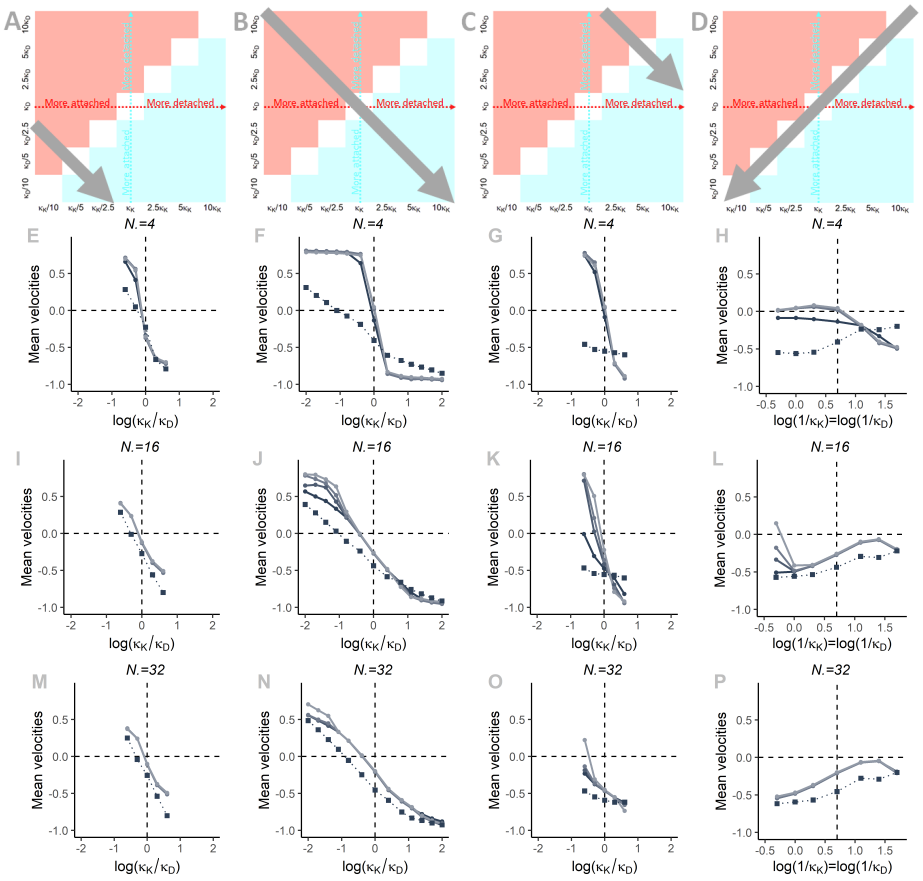

Figure 8: Mean velocities of the 150 filaments as functions of dissociation constants ratios. (A-D) Grey arrows indicated from which regions dissociation constant are taken to compute ratios for each column. Row 2, 3 and 4 show results for $N_\bullet = 4$, 16 and 32. (E, I and M) Both types of motors have dissociation constants smaller than their base values (strong affinities for both motors). (F, J an N) One type with $\kappa_\bullet$ smaller than its base value and the other with $\kappa_\bullet$ larger than its base value (one type with a strong affinity and the other with a weak one). (G, K and O) Both types of motors have dissociation constants larger than their base values (weak affinities for both motors). (H, L and P) Both types have the same affinity (from smaller to larger affinities). Dotted lines with squares represent results from the deterministic description and plain lines with dots are results from the stochastic description at different times from 10 seconds (the darkest tone) to 550 seconds (the lightest tone). Parameter values used for simulations are provided in Table 1.

motors in cells – extrinsic noise) on the filament motions. Our finding goes in the same direction as [37], which shows that stochastic effects are found to dominate the dynamics when a small number of motors is attached to the cargo. In [37], the cargo is a single bead. Furthermore, the presence of noise increases the performances of the weakest motor as random events allow the strongest motors to detach giving the weaker motors a chance to attach again and establish.

Our model is another illustration of Keizer's paradoxe [24, 25], which refers to the existence of discrepancy between the long-time behaviour obtained with the deterministic and stochastic description. This discrepancy results from the differences in timescales and types of "attractors" existing between both formalisms. Stochastic fluctuations can perturb significantly the deterministic equilibria, slowing down the stabilization process and allowing to find global attractors amongst the local ones found with the deterministic description [51].

The biological interpretation of our conclusions is that the initial distribution of motors in cells does not play an important role in the intracellular transport as the stochastic fluctuations related to motors attachment and detachment processes will make their effects fade. In other words, the intrinsic noise annihilates the extrinsic noise. The presence of the intrinsic noise makes the motor-cargo interaction affinities the main regulators of the filament ensemble transport and organizes it by synchronizing the direction of motions of all filaments. The fewer binding sites, the most efficient is the synchronization. Furthermore, no strong motor-cargo interactions for both types are preferable for a more efficient regulation allowing small differentials in motor-cargo affinities to switch the net transport direction. Hence, a "good strategy" for an efficacious transport of intermediate filaments in cells, easy to regulate, would be to maintain a few binding sites on intermediate filaments with no strong affinities to motors. These qualitative predictions will have to be tested experimentally.

Acknowledgments

SP was supported by a Discovery Grant of the Natural Sciences and Engineering Research Council of Canada (RGPIN-2018-04967) and a Burroughs Wellcome Fund 2020 Collaborative Research Travel Grant. SEM and CL were supported by the Pasteur Institute (Paris, France) and the National Center for Scientific Research (CNRS). SEM was supported by the La Ligue contre le cancer (S-CR17017). CL was supported by a French National Research Agency grant (ANR 16-CE13-019).

Appendix A. Additional computational results

Figure A.9 gives complete results of Figure 4 for the 49 pairs of dissociation constants as described in Figure 2.

Figure A.10 aggregate data from Figure 7 for four cases: different strong affinities for both motors, one type with a strong affinity and the other with a weak one, different weak affinities for both motors and same affinity for both types. Proportions of retrograde and anterograde filaments obtained with both the deterministic and stochastic formalisms are plotted as functions of ratios of dissociation constants κ_K/κ_D.

References

[1] J. Dallon, C. Leduc, S. Etienne-Manneville, S. Portet, Stochastic modeling reveals how motor protein and filament properties affect intermediate filament transport, Journal of Theoretical Biology 464 (2019) 132–148.

[2] S. Portet, C. Leduc, S. Etienne-Manneville, J. Dallon, Deciphering the transport of elastic filaments by antagonistic motor proteins, Phys. Rev. E 99 (2019) 042414.

[3] S. Etienne-Manneville, Cytoplasmic intermediate filaments in cell biology, Annual Review in Cell and Developmental Biology 34 (2018).

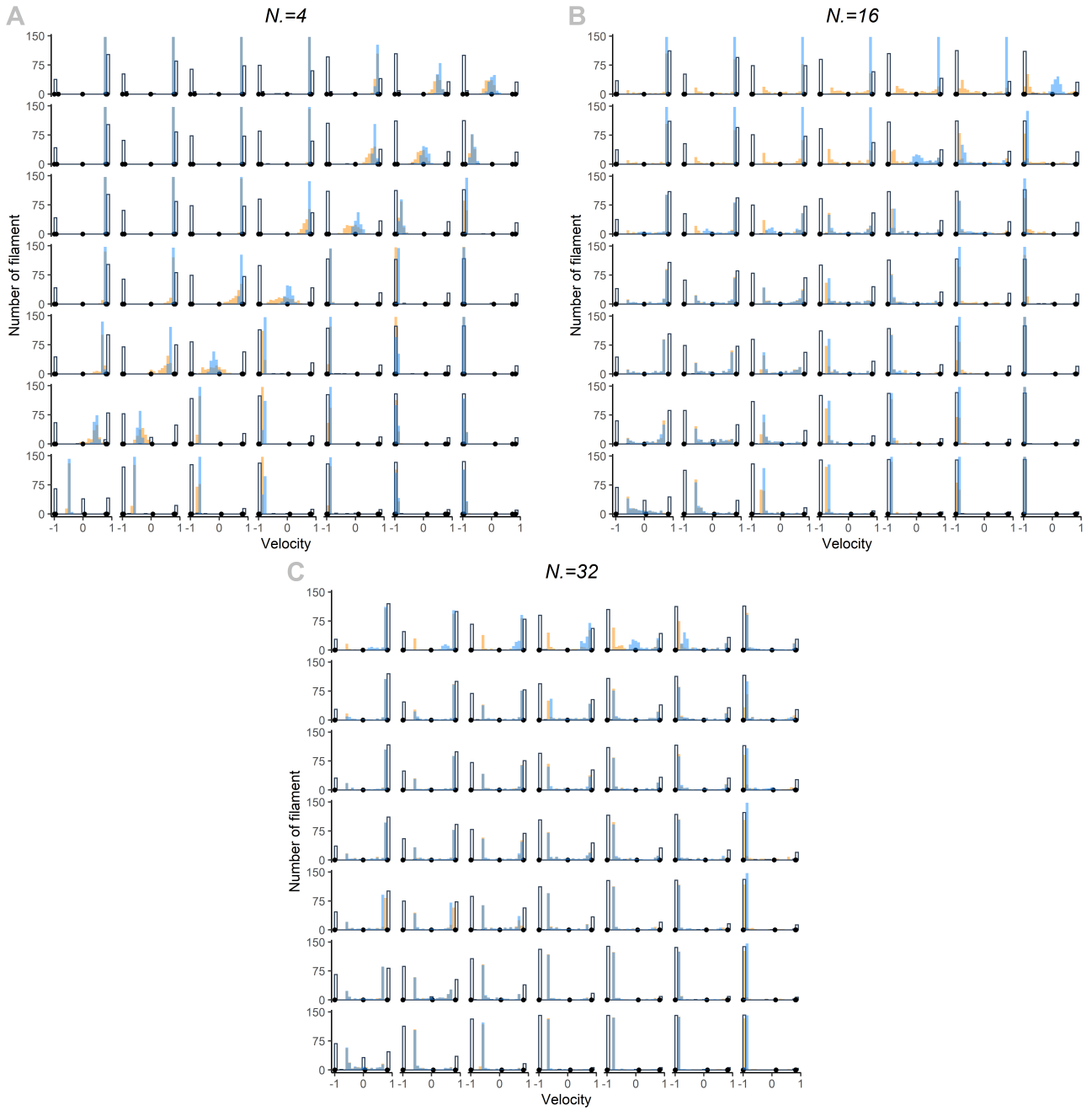

Figure A.9: Distributions of the individual velocities reached by the 150 filaments with the deterministic formalism (white bars), with the stochastic formalism at $T = 10$ seconds (in orange) and $T = 550$ seconds (in blue) for 49 pairs of κ. with $N. = 4$ (A), 16 (B) and 32 (C). Black dots are the (stable and unstable) equilibrium values v^* satisfying $0 = (1 - v^*/v_{0K})\frac{N_K F_{sK}}{1+\kappa_K f_K(v^*)} + (1 + v^*/v_{0D})\frac{N_D F_{sD}}{1+\kappa_D f_D(v^*)} + v^*\mu$ [2].

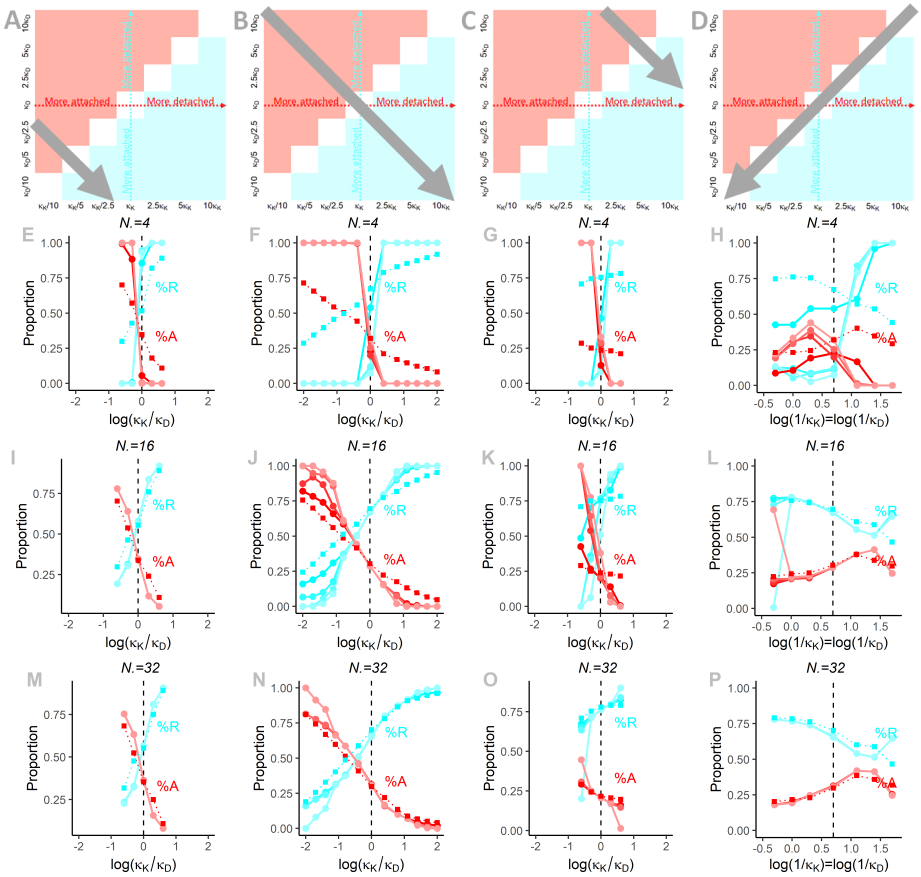

Figure A.10: Proportions of filaments moving retrogradely (in cyan tones) and anterogradely (in red tones) as functions of the ratio of dissociation constants. Proportions of slow filaments are not represented for figure readability. (A-D) Grey arrows indicated from which regions dissociation constant are taken to compute ratios for each column. Row 2, 3 and 4 show results for $N_{\cdot}$ =4, 16 and 32. (E, I and M) Both types of motors have dissociation constants smaller than their base values (strong affinities for both motors). (F, J and N) One type with $\kappa_{\cdot}$ smaller than its base value and the other with $\kappa_{\cdot}$ larger than its base value (one type with a strong affinity and the other with a weak one). (G, K and O) Both types of motors have dissociation constants larger than their base values (weak affinities for both motors). (H, L and P) Both types have the same affinity (from smaller to larger affinities). Dotted lines with squares represent results from the deterministic description and plain lines with dots are results from the stochastic description at different times from 10 seconds (the darkest tone) to 550 seconds (the lightest tone). Parameter values used for simulations are provided in Table 1.

[4] C. Leduc, S. Etienne-Manneville, Regulation of microtubule-associated motors drives intermediate filament network polarization, Journal of Cell Biology 216 (2017) 1689–1703.

[5] S. Portet, A. Madzvamuse, A. Chung, R. E. Leube, R. Windoffer, Keratin dynamics: modeling the interplay between turnover and transport, PloS One 10 (2015) e0121090.

[6] F. Gyoeva, V. Gelfand, Coalignment of vimentin intermediate filaments with microtubules depends on kinesin, Nature 353 (1991) 445–448.

[7] B. T. Helfand, L. Chang, R. D. Goldman, Intermediate filaments are dynamic and motile elements of cellular architecture, Journal of Cell Science 117 (2004) 133–141.

[8] C. Hookway, L. Ding, M. W. Davidson, J. Z. Rappoport, G. Danuser, V. I. Gelfand, Microtubule-dependent transport and dynamics of vimentin intermediate filaments, Molecular Biology of the Cell 26 (2015) 1675–1686.

[9] R. E. Leube, M. Moch, R. Windoffer, Intracellular motility of intermediate filaments, Cold Spring Harbor Perspectives in Biology 9 (2017).

[10] A. B. Kolomeisky, M. E. Fisher, Molecular motors: a theorist's perspective, Annu Rev Phys Chem 58 (2007) 675–95.

[11] A. B. Kolomeisky, Motor proteins and molecular motors: how to operate machines at the nanoscale, Journal of Physics: Condensed Matter 25 (2013) 463101.

[12] P. Xie, Insight into the chemomechanical coupling mechanism of kinesin molecular motors, Communications in Theoretical Physics (2021).

[13] C. M. Johnson, J. D. Fenn, A. Brown, P. Jung, Dynamic catch-bonding generates the large stall forces of cytoplasmic dynein, Physical biology 17 (2020) 046004.

[14] M. E. Fisher, A. B. Kolomeisky, Simple mechanochemistry describes the dynamics of kinesin molecules, Proceedings of the National Academy of Sciences 98 (2001) 7748–7753.

[15] P. J. Atzberger, C. S. Peskin, A brownian dynamics model of kinesin in three dimensions incorporating the force-extension profile of the coiled-coil cargo tether, Bulletin of mathematical biology 68 (2006) 131–160.

[16] S.-K. Guo, P.-Y. Wang, P. Xie, A model of processive movement of dimeric kinesin, J Theor Biol 414 (2017) 62–75.

[17] L. Trott, M. Hafezparast, A. Madzvamuse, A mathematical understanding of how cytoplasmic dynein walks on microtubules, Royal Society open science 5 (2018) 171568.

[18] A. Kunwar, S. K. Tripathy, J. Xu, M. K. Mattson, P. Anand, R. Sigua, M. Vershinin, R. J. McKenney, C. Y. Clare, A. Mogilner, et al., Mechanical stochastic tug-of-war models cannot explain bidirectional lipid-droplet transport, Proceedings of the National Academy of Sciences 108 (2011) 18960–18965.

[19] A. Kunwar, A. Mogilner, Robust transport by multiple motors with nonlinear force–velocity relations and stochastic load sharing, Physical biology 7 (2010) 016012.

[20] M. J. Müller, S. Klumpp, R. Lipowsky, Tug-of-war as a cooperative mechanism for bidirectional cargo transport by molecular motors, Proceedings of the National Academy of Sciences 105 (2008) 4609–4614.

[21] M. J. Müller, S. Klumpp, R. Lipowsky, Bidirectional transport by molecular motors: enhanced processivity and response to external forces, Biophysical Journal 98 (2010) 2610–2618.

[22] W. O. Hancock, Bidirectional cargo transport: moving beyond tug of war, Nature Reviews Molecular Cell Biology 15 (2014) 615.

[23] M. Vellela, H. Qian, A quasistationary analysis of a stochastic chemical reaction: Keizer's paradox, Bulletin of mathematical biology 69 (2007) 1727—1746.

[24] P. Childs, J. P. Keener, Slow manifold reduction of a stochastic chemical reaction: Exploring keizer's paradox, Discrete and Continuous Dynamical Systems - B 17 (2012) 1775–1794.

[25] J. Keizer, Statistical Thermodynamics of Nonequilibrium Processes, 1987.

[26] J. R. Kardon, S. L. Reck-Peterson, R. D. Vale, Regulation of the processivity and intracellular localization of saccharomyces cerevisiae dynein by dynactin, Proceedings of the National Academy of Sciences 106 (2009) 5669–5674.

[27] T. Korten, S. Diez, Setting up roadblocks for kinesin-1: mechanism for the selective speed control of cargo carrying microtubules, Lab Chip 8 (2008) 1441–1447.

[28] I. A. Telley, P. Bieling, T. Surrey, Obstacles on the microtubule reduce the processivity of kinesin-1 in a minimal in vitro system and in cell extract, Biophysical journal 96 (2009) 3341–3353.

[29] J. D. Fenn, C. M. Johnson, J. Peng, P. Jung, A. Brown, Kymograph analysis with high temporal resolution reveals new features of neurofilament transport kinetics, Cytoskeleton 75 (2017) 22–41.

[30] A. Robert, P. Tian, S. A. Adam, M. Kittisopikul, K. Jaqaman, R. D. Goldman, V. I. Gelfand, Kinesin-dependent transport of keratin filaments: a unified mechanism for intermediate filament transport, FASEB Journal 33 (2019) 00–00.

[31] Z. Qin, L. Kreplak, M. J. Buehler, Hierarchical structure controls nanomechanical properties of vimentin intermediate filaments, PLOS ONE 4 (2009) 1–14.

[32] Z. Qin, M. J. Buehler, L. Kreplak, A multi-scale approach to understand the mechanobiology of intermediate filaments, Journal of Biomechanics 43 (2010) 15–22. Special Issue on Cell Mechanobiology.

[33] J. Block, H. Witt, A. Candelli, E. J. Peterman, G. J. Wuite, A. Janshoff, S. Köster, Nonlinear loading-rate-dependent force response of individual vimentin intermediate filaments to applied strain, Physical Review Letters 118 (2017) 048101.

[34] C. Guzman, S. Jeney, L. Kreplak, S. Kasas, A. Kulik, U. Aebi, L. Forro, Exploring the mechanical properties of single vimentin intermediate filaments by atomic force microscopy, Journal of Molecular Biology 360 (2006) 623–630.

[35] L. Kreplak, D. Fudge, Biomechanical properties of intermediate filaments: from tissues to single filaments and back, BioEssays 29 (2007) 26–35.

[36] Z. Qin, C.-C. Chou, L. Kreplak, M. Buehler, Structural, mechanical and functional properties of intermediate filaments from the atomistic to the cellular scales, in: S. Li, B. Sun (Eds.), Advances in Cell Mechanics, Springer, 2011, pp. 139–140.

[37] A. Kunwar, A. Mogilner, Robust transport by multiple motors with nonlinear force–velocity relations and stochastic load sharing, Physical Biology 7 (2010) 16012.

[38] S. Klumpp, R. Lipowsky, Cooperative cargo transport by several molecular motors, Proceedings of the National Academy of Sciences 102 (2005) 17284–1789.

[39] P. Xie, Theoretical analysis of dynamics of kinesin molecular motors, ACS Omega 5 (2020) 5721–5730.

[40] D. Pischel, K. Sundmacher, R. J. Flassig, Efficient simulation of intrinsic, extrinsic and external noise in biochemical systems, Bioinformatics 33 (2017) i319–i324.

[41] K. Soetaert, T. Petzoldt, R. W. Setzer, Solving differential equations in R: Package deSolve, Journal of Statistical Software 33 (2010) 1–25.

[42] C. Leduc, O. Campàs, K. B. Zeldovich, A. Roux, P. Jolimaitre, L. Bourel-Bonnet, B. Goud, J.-F. Joanny, P. Bassereau, J. Prost, Cooperative extraction of membrane nanotubes by molecular motors, Proceedings of the National Academy of Sciences 101 (2004) 17096–17101.

[43] C. Leidel, R. A. Longoria, F. M. Gutierrez, G. T. Shubeita, Measuring molecular motor forces in vivo: implications for tug-of-war models of bidirectional transport, Biophysical Journal 103 (2012) 492–500.

[44] S. Sudhakar, M. K. Abdosamadi, T. J. Jachowski, M. Bugiel, A. Jannasch, E. Schäffer, Germanium nanospheres for ultraresolution picotensiometry of kinesin motors, Science 371 (2021).

[45] J. G. De La Torre, C. Lopez, Dimensions of short, rodlike macromolecules from, Biopolymers 23 (1984) 611–615.

[46] C. M. Johnson, J. D. Fenn, A. Brown, P. Jung, Dynamic catch-bonding generates the large stall forces of cytoplasmic dynein, Physical Biology 17 (2020) 046004.

[47] S. Toba, T. M. Watanabe, L. Yamaguchi-Okimoto, Y. Y. Toyoshima, H. Higuchi, Overlapping hand-over-hand mechanism of single molecular motility of cytoplasmic dynein, Proceedings of the National Academy of Sciences 103 (2006) 5741–5745.

[48] J. Atherton, J. J. Hummel, N. Olieric, J. Locke, A. Peña, S. S. Rosenfeld, M. O. Steinmetz, C. C. Hoogenraad, C. A. Moores, The mechanism of kinesin inhibition by kinesin-binding protein, eLife 9 (2020) e61481.

[49] J. T. Kevenaar, S. Bianchi, M. van Spronsen, N. Olieric, J. Lipka, C. P. Frias, M. Mikhaylova, M. Harterink, N. Keijzer, P. S. Wulf, M. Hilbert, L. C. Kapitein, E. de Graaff, A. Ahkmanova, M. O. Steinmetz, C. C.

Hoogenraad, Kinesin-binding protein controls microtubule dynamics and cargo trafficking by regulating kinesin motor activity, Current biology : CB 26 (2016) 849—861.

[50] N. Korabel, T. A. Waigh, S. Fedotov, V. J. Allan, Non-markovian intracellular transport with sub-diffusion and run-length dependent detachment rate, PLOS ONE 13 (2018) 1–23.

[51] Y. Zhang, H. Ge, H. Qian, One-dimensional birth-death process and delbrück-gillespie theory of mesoscopic nonlinear chemical reactions, Studies in Applied Mathematics 129 (2012) 328–345.

[52] D. F. Anderson, G. A. Enciso, M. D. Johnston, Stochastic analysis of biochemical reaction networks with absolute concentration robustness, J. R. Soc. Interface. 11 (2014) 20130943.